Available online at www.sciencedirect.com
SCIENCE DIRECT
Journal of Theoretical Biology 241 (2006) 903–918
Journal of Theoretical Biology
www.elsevier.com/locate/yjtbi

Vascular network remodeling via vessel cooption, regression and growth in tumors

K. Bartha[a], H. Rieger[b,*]

[a]Department of Medical Biochemistry, Semmelweis University, Budapest, Hungary
[b]Theoretische Physik, Fachrichtung 7.1, Universität des Saarlandes, PF 151150, 66041 Saarbrücken, Germany

Received 19 August 2005; received in revised form 23 January 2006; accepted 23 January 2006
Available online 20 March 2006

Abstract

The transformation of the regular vasculature in normal tissue into a highly inhomogeneous tumor specific capillary network is described by a theoretical model incorporating tumor growth, vessel cooption, neo-vascularization, vessel collapse and cell death. Compartmentalization of the tumor into several regions differing in vessel density, diameter and in necrosis is observed for a wide range of parameters in agreement with the vessel morphology found in human melanoma. In accord with data for human melanoma the model predicts that microvascular density (MVD), regarded as an important diagnostic tool in cancer treatment, does not necessarily determine the tempo of tumor progression. Instead it is suggested that the MVD of the original tissue as well as the metabolic demand of the individual tumor cell plays the major role in the initial stages of tumor growth.

Keywords: Vascular networks; Tumor growth; Blood flow; Angiogenic modeling; Cancer

1. Introduction

Tumor induced angiogenesis is the formation of new blood vessels around the tumor microenvironment for supporting expansion of the tumor mass (Hanahan and Folkman, 1996). Tumor vessels can arise by angiogenic sprouting (Folkman et al., 1971), intussusception (Burri et al., 2004), or by recruiting endothelial precursor cells from the bone marrow (Lyden et al., 2001). In addition, tumor cells may also co-opt existing blood vessels from the host (Holash et al., 1999a).

Tumor growth strictly depends on adequate supply of oxygen (O_2) through blood vessels. Vascularization determines pathophysiological characteristics of the tumors, such as tumor invasiveness and metastasis formation. Moreover successful therapy critically depends on the transvascular delivery and permeability of larger molecules into the tumor tissue. Therefore quantification various aspects of the tumor vasculature provides valuable tools for tumor prognosis.

However, the degree of vascularization is not homogeneous, it depends on the net balance between proangiogenic and antiangiogenic factors stimulating and inhibiting vessel growth respectively, as well as on non-angiogenic factors, such as O_2 and nutrient consumption rates of tumor cells. Recently also the effect of the host microenvironment in the tumor circulation was fully realized (Fukumura et al., 1997). The molecular components involved in tumor induced vascularization include hypoxia-inducible transcription factors, which trigger a coordinated response of angiogenesis by inducing expression of growth factors (GF) (Maxwell et al., 1997; Plate and Risau, 1995). Individual tumors can produce a variety of proangiogenic GFs, among which members of vascular endothelial growth factor (VEGF) and angiopoietin family have a predominant role, all inducing endothelial cell differentiation, proliferation and increase in vessel length [reviewed in: (Carmeliet and Jain, 2000)]. VEGF also exerts morphogenic activity by increasing luminal diameter of existing vessels (Zhou et al., 1998). Angiogenic inhibitors, suppressing proliferation and migration of endothelial cells include thrombospondin-1 (Jimenez et al., 2000), angiostatin (O'Reilly et al., 1994) and endostatin (O'Reilly et al.,

*Corresponding author. Tel.: +49 681 302 3969; fax: +49 681 302 4899.
E-mail address: h.rieger@mx.uni-saarland.de (H. Rieger).

0022-5193/$ - see front matter © 2006 Elsevier Ltd. All rights reserved.
doi:10.1016/j.jtbi.2006.01.022

1997). They are produced either by the tumor or by the host stromal cells (Fears et al., 2005), cause endothelial cell apoptosis and may be involved in tumor dormancy.

Increased cellular proliferation in tumors also results in a switch from O_2 consuming to glycolytic pathways providing tumor cells with an alternative energy source during low O_2 supply (Iyer et al., 1998; Minchenko et al., 2002). However, each tumor has a minimum O_2 consumption rate, characteristic for its metabolic demand, below which tumor cells loose viability, the rate varying with tissue origin and with tumor progression. Thus the minimum O_2 and nutrient consumption will limit how far away from the vasculature tumor cells can remain viable, the number of viable tumor cell and their GF production in turn will regulate vascular density, blood flow, and permeability.

Tumor vessels are abnormal in many ways, they show uncontrolled permeability, are tortuous and dilated, have excessive branching, shunts and undergo constant regression and remodeling. This may be due to an imbalance of angiogenic regulators such as VEGF and angiopoietins, giving rise to chaotic blood flow, unstable, leaky vessels (Maisonpierre et al., 1997). The tumor endothelium has widened inter-endothelial junctions, discontinuous or absent basement membrane with loosely associated mural cells (Hashizume et al., 2000). In addition to regulatory mechanisms achieved by angiogenic factors and structural properties of the vessel wall, haemodynamic conditions, especially flow and shear stress (Cullen et al., 2002; Milkiewicz et al., 2001), play a decisive role in maintaining high vascular permeability, inhomogeneous diameter, and concomitant collapse typically observed with tumor blood vessels. Other factors leading to frequently observed vessel collapses in tumors are decreased intravascular pressure and increased interstitial pressure (Boucher and Jain, 1992) and solid stress generated by the growing tumor itself (Griffon-Etienne et al., 1999). It is also generally acknowledged, that increase in blood flow contribute to vessel enlargement in any vessel, whereas disturbed flow or severe reduction of blood flow is associated with apoptosis of endothelial cells and vessel regression (Dimmeler and Zeiher, 2000).

Although recent insights in the molecular basis of angiogenesis have resulted in the discovery of many new angiogenic molecules, many questions remain unsolved. So far very little is known about the spatial cues guiding endothelial cells into correct patterns and three-dimensional networks. One of the basic questions is: whether the quantification of some aspects of the vascular network formation can make predictions for tumor progression in patients and if yes, what are these aspects.

From what we have described so far it appears that a theoretical model describing quantitatively the dynamics of the remodeling process of the vascular network during tumor growth should contain at least the following aspects: (1) a pre-existing network representing the normal vasculature that can be modified dynamically via growth, regression and modification of its links (representing blood vessels), (2) a nucleus of tumor cells that can proliferate, age and die, (3) at least two concentration fields: one whose sources are the vessels of the network and represents oxygen and other nutrients, and one whose sources are the tumor cells and which represent GFs, (4) a model for the hemodynamic flow within the network, (5) a specific set of dynamical rules that describe (a) the process of interaction between vessels and tumor cells mediated by the two concentration fields and (b) the influence of the blood flow. One intention of our paper is to show that a number of phenomena, like the systematic compartmentalization of the tumor into rapidly vascularizing periphery and necrotic regions and other morphological details of tumor vasculature are already a consequence of the aforementioned five inputs.

Previous attempts to describe mathematically the growth of tumor vasculature either focused on a particular model for angiogenesis in presence of a GF source alone (Anderson and Chaplain, 1998; Levine et al., 2001) or studied tumor growth within a vascular network of fixed topology but with hydrodynamically generated inhomogeneities (Alarcón et al., 2003). From a theoretical point of view the tumor/vessel system appears as a dynamically evolving weighted network or graph with a hydrodynamic flow imprinted on it, plus a non-trivial growth process (including birth and death) in continuous or discrete time and space, both interacting non-locally via several diffusion fields. This is a rather complex system which we intend to analyse numerically by computer simulations. We define the model in the next section in terms of the elementary stochastic processes, which in principle can be formulated in terms of a Master equation (Van Kampen, 1992). We implemented it as a Monte-Carlo simulation on a computer and we present and discuss the results in the subsequent sections.

2. Definition of the model

A clinical case of a human melanoma type tumor was chosen (Döme et al., 2002) as the experimental basis of the theoretical model and other selected experimental data available from solid tumors are also involved. In the model we assume, that tumor induced neovascularization starts with two parallel processes, cooption of existing vessels and vessel sprouting. We do not consider recruiting endothelial cells from the bone marrow.

A hybrid probabilistic cellular automaton model is defined on a square lattice with $N = L^2$ sites with coordinates $\mathbf{r} = (n_x\Delta r,\ n_y\Delta r)$, $n_x, n_y \in \{1,\ldots,L\}$ and in discrete time $\tau = n\Delta\tau$, with $n = 0,1,2,\ldots$ Each site represents an area Δr^2 with $\Delta r = 10\,\mu\text{m}$, which is approximately the size of a single endothelial cell (EC) or tumor cell (TC), and each time step represents a time interval of length $\Delta\tau$. Table 1 lists the dynamical variables that define the state of each site at time τ. For instance $e(\mathbf{r},\tau) = 1$ (or 0) means that a vessel segment is present (or absent) at site $\mathbf{r}$ and time τ, its radius (if present) is given by $e_r(\mathbf{r},\tau)$, its blood flow rate by $e_Q(\mathbf{r},\tau)$ and its wall shear stress value $e_f(\mathbf{r},\tau)$. If $t(\mathbf{r},\tau) = 1$

Table 1
Variables defining the state at site $\mathbf{r}$ at time τ

e	0/1: EC or vessel absent/present
e_r	$\in[0,r_{\max}]$, radius of vessel
e_Q	$\geqslant 0$, blood flow rate through vessel segment
e_f	$\geqslant 0$, shear stress on vessel wall
t	0/1 : TC absent/present
t_{uO}	$\in[0,T_{\max}]$, time of TC in underoxygenated state
c_{oxy}	$\geqslant 0$; oxygen concentration field
c_{GF}	$\geqslant 0$; growth factor concentration field

Table 2
Model parameters

Δr	lattice constant: space discretization	10 μm
$\Delta\tau$	length of time step: time discretization	1 h
MVD_0	original MVD	$100/\mathrm{mm}^2$
TC_0	original tumor size	10^3–10^5
R_{GF}	growth factor diffusion radius	~100–400 μm
R_{oxy}	oxygen diffusion radius	~100–150 μm
θ_{GF}	growth factor threshold	10^{-3}–10^{-1}
$\theta_{oxy,EC}$	oxygen threshold for Ecs	10^{-2}–10^{-1}
$\theta_{oxy,TC}$	oxygen threshold for TCs	$0.1\cdot\theta_{oxy,EC}$
T_t	TC proliferation time	$10\Delta\tau = 10$ h
T_e	EC proliferation time	$40\Delta\tau = 40$h
R_0	initial vessel radius	$1\Delta r = 10$ μm
r_{max}	maximum vessel radius	$3.5r_0 = 35$ μm
M_{max}	maximum sprout migration distance	$10\Delta r = 100$ μm
$T_{collapse}$	collapse time of critical vessels	10–$100T_e$
f_{crit}	critical shear stress on vessel walls	0.2–0.8 f_0
T_{uO}	maximum TC survival time in hypoxia	$100\Delta\tau = 100$ h

(or 0) TCs are present (or absent) at site $\mathbf{r}$ and time τ, $t_{uO}(\mathbf{r},\tau)$ is the time it spent in an underoxygenated state. GF and O_2 concentration at site $\mathbf{r}$ and time τ are given by $c_{GF}(\mathbf{r},\tau)$ and $c_{oxy}(\mathbf{r},\tau)$, respectively. In each time step these variables are modified probabilistically according to the rules described below, which depend on various fixed parameters listed in Table 2.

The initial state of the system at $\tau = 0$ represents a regularly vascularized region of a given micro-vascular density MVD_0 with a small tumor in the center: vessels are arranged in a regular pattern, which for simplicity is chosen to be a "Manhattan network" (a regular mesh in two dimensions) with a lattice constant a. This means that $e(\mathbf{r},\tau=0) = 1$ and $e_r(\mathbf{r},\tau=0) = r_0$ for $\mathbf{r} = (na,y)$ and $\mathbf{r} = (x,na)$ with $n = 0,1,2,\ldots,L/a$ and $x,y = 0,1,2,\ldots,L$. All other sites have $e(\mathbf{r},\tau=0) = 0$. For the initial tumor it is $t(\mathbf{r},\tau=0) = 1$ in a region containing TC_0 sites determined probabilistically according to the Eden growth rule (Eden, 1961), where starting from a single TC at the center successively a surface site of the tumor is randomly chosen and occupied by a TC until the tumor consists of TC_0 cells.

In the next time step, and in all subsequent time steps, the following computations are performed one after the other in a Monte Carlo simulation, yielding the new system state at time $\tau+\Delta\tau$, which is evaluated for several quantities of interest. The simulation is stopped either if the tumor reaches the system boundary or if it ceases to exist (depending on the chosen parameter values). We did not incorporate any mechanism resulting in the inhibition or arrest of tumor growth here.

Definition of the GF concentration field $c_{GF}(\mathbf{r},\tau)$: Each TC synthesizes a certain amount of GF and the sum of GF secreted creates a GF concentration field around the tumor. GF (e.g. VEGF) expression is known to be regulated under hypoxic conditions in TC-s (Plate et al., 1992; Shweiki et al., 1992) suggesting that GF concentration might depend on synthesis rate around various TC sites, but the existence of a matrix storage pools for GF (Goerges and Nugent, 2004) would rather predict a generation of a preformed GF gradient in the very close vicinity of TC-s. Therefore in our model we defined GF concentration in such a way, that it is a final result of all TC processes, hypoxia as well as genetic alterations (Semenza, 2003):

$$c_{GF}(\mathbf{r},\tau) = \sum\nolimits_{\{\mathbf{r}' \text{ with } t(\mathbf{r}',\tau)=1\}} f_{\mathrm{GF}}(|\mathbf{r}-\mathbf{r}'|),$$

where the sum is over all TCs at time τ. The contribution $f_{GF}(|\mathbf{r}-\mathbf{r}'|)$ of each TC to the GF pool is assumed to decrease linearly to zero within a distance R_{GF}: $f_{GF}(r) = (R_{GF}-r)/N$ for $r \leqslant R_{GF}$ and $f_{GF}(r) = 0$ for $r > R_{GF}$ and the normalization N chosen such that $\Sigma_{\mathbf{r}} f_{GF}(|\mathbf{r}|) = 1$. The linear shape of $f_{GF}(r)$ is a numerically convenient and sufficiently good approximation to the exact (exponentially decaying) Greens-function for the diffusion problem with a point-source of unit strength (representing a single TC) and spatially constant decay rate (representing a constant GF consumption and/or degradation in the extra-cellular matrix).

An additional hypoxia dependence of GF production can also be incorporated into our model by restricting the sum over TCs in the above definition of $c_{GF}(\mathbf{r},\tau)$ to TCs that are underoxygenated, i.e. to sites $\mathbf{r}'$ with $c_{oxy}(\mathbf{r}',\tau) < \theta_{oxy}$, or giving them a large GF source strength. We study this variant of our model in a forthcoming publication (Bartha and Rieger, 2006).

In principle the diffusion of GF into the matrix is a time dependent process which causes a delay in the change of concentration at a distance when the tumor configuration changes. Since the time scale governing this process is much shorter than the time scale on which TCs proliferate and/or die, we assume that the process reaches its stationary state within the time interval $\Delta\tau$ and approximate the emerging concentration profile around each source in the aforementioned way.

Identification of circulated sites $S_{circ}(\tau)$: For each vessel segment (i.e. each site $\mathbf{r}$ with $e(\mathbf{r},\tau) = 1$) it is checked whether it is located on an uninterrupted path in the current vessel network that connects the sites (0,0) and (L,L). Technically this check is performed by computing the bi-connected components (Tarjan, 1972) of the graph underlying the vessel network. If this condition is fulfilled, blood can flow through this vessel and $\mathbf{r}$ is a member of the set of circulated vessels $S_{circ}(\tau)$.

Definition of the oxygen concentration field $c_{oxy}(\mathbf{r},\tau)$: Intensive cellular proliferation in tumors results in an increase in oxygen demand, TC-s remain viable within a certain radius around a vessel, generating "cuff"-s on the available oxygen concentration field (Hlatky et al., 2002). However the maximal radius of oxygen concentration field, that still supports TC proliferation ("cuff size") depends both on the oxygen concentration released from a vessel and on the consumption of oxygen by TC-s, modeled by an oxygen concentration threshold θ_{oxy} defined below. For simplicity we do not calculate $c_{oxy}(\mathbf{r},\tau)$ via the stationary solution of a diffusion equation with vessels as sources and TCs as sinks, but assume that the O_2 supply of individual vessel segments depends mainly on circulation.

$$c_{oxy}(\mathbf{r},\tau)=\sum\nolimits_{\{\mathbf{r}'\in S_{circ}(\tau)\}} f_{oxy}(|\mathbf{r}-\mathbf{r}'|),$$

where $f_{oxy}(r)=(R_{oxy}\text{-}r)/N'$ for $r\leqslant R_{oxy}$ and $f_{oxy}=0$ for $r>R_{oxy}$. The normalization constant N' is chosen such that $\Sigma_{\mathbf{r}} f_{oxy}(|\mathbf{r}|)=1$. Oxygen diffusion through the matrix is, as GF diffusion, a time dependent process which causes a delay in the change of concentration at a distance when the vessel configuration changes. The diffusion constant of O_2 is of the order of 2.4×10^{-5} cm^2/s, which means that in the time scale of $\Delta\tau=1$ h the O_2-diffusion process is in a quasi stationary regime. The precise O_2-concentration profile around each vessel will also depend on the presence of sinks (e.g. TCs) but an approximation through a linear profile around each segment is sufficient for our purposes here. We assume here a constant source strength of each vessel segment, which overestimates the oxygen concentration in regions of increased MVD since oxygen diffuses passively and is driven by concentration gradients. In principle the source strengths should be determined implicitly along the lines of (Secomb et al., 2004), but this becomes numerically very hard for large system sizes, as is the solution of the oxygen diffusion problem treatment using finite difference methods (Alarcón et al., 2003).

Blood flow and shear stress computation: The shear stress exerted by the blood flow upon the vessel walls is considered to be a principal stimulus for EC-s, the primary driving force for vessel architecture (Davies, 1995; Ishida et al., 1997). For a given vessel network we identify the vessel segment with cylindrical tubes of radius $e_r(\mathbf{r},\tau)$ and approximate the flow through it by laminar steady Poiseuille flow of a homogeneous liquid. We neglect here the fact that blood is an inhomogeneous fluid which is commonly modeled by a radius dependent viscosity. We also neglect a structural adaptation mechanism of the vessels as well as haematocrit (for a proper treatment of these details in a fixed vessel network see Alarcón et al., 2003). For laminar pipe flow the flow rate is determined by the pressure drop ΔP between the end points of the segments according to Poiseuilles law:

$$e_q(\mathbf{r},\tau)=q/\Delta\tau=\text{const}\cdot e_r^4(\mathbf{r},\tau)\Delta P,$$

where const $=\pi/(8\eta(e_r)L(e))$, with $\eta(e_r)$ the blood viscosity in a vessel of radius e_r and $L(e)$ the length of the vessel e. Because vessel segments in our model all have the same length, $L(e)=\Delta r$, and the viscosity η is assumed to be radius independent the factor const is indeed constant, i.e. independent of the vessel under consideration.

The boundary conditions for the pressure are defined in such a way that a homogeneous flow distribution in the vessels of the original network arises: The pressure in the vessel segments decreases linearly on the boundary vessels from $P_{\max}$ at $\mathbf{r}=(0,0)$ to $(P_{\max}-P_{\min})/2$ at $\mathbf{r}=(L,0)$ and $\mathbf{r}=(0,L)$, and from there from $(P_{\max}-P_{\min})/2$ to $P_{\min}$ at $\mathbf{r}=(L,L)$, resulting in homogeneous global net flow in the diagonal direction. Since only pressure differences enter the flow equations $P_{\max}$ and $P_{\min}$ can be chosen arbitrarily and are set to 1 and 0, respectively, in arbitrary units. Using Kirchhoff's law we calculate the pressure drop and flow in each vessel segment, which is numerically demanding but otherwise standard in vascular network models (Gödde and Kurz, 2001; McDougall et al., 2002). Ideal pipe flow furthermore implies that the shear stress $e_f(\mathbf{r},\tau)$ acting upon the vessel walls of each vessel is given by

$$e_f(\mathbf{r},\tau)=\text{const}'e_r(\mathbf{r},\tau)\Delta P,$$

where const$'=1/2L(e)$, which is a constant.

The following dynamical processes involving growth and removal of TCs and vessels are incorportaed into our model, as is sketched in Fig. 1.

TC proliferation: (Fig. 1a) It is assumed that only TCs with at least one free neighbor site can proliferate. This implies that the TCs are assumed to be incompressible and excludes internal tumor growth. Experimental data for real tumors indicate that TC proliferation is indeed confined to the outer rim of the tumor (Brú et al., 2003): although TCs are elastic and proliferation can also take place within the tumor, after an initial exponential growth regime the displacement of existing normal tissue will build up solid stress inside the tumor that confines the TC proliferation to the outer rim of the tumor (Drasdo and Höme, 2005). This is the regime we focus on here.

If the local O_2 concentration $c_{oxy}(\mathbf{r})$ at such a tumor surface site $\mathbf{r}$ exceeds a threshold θ_{oxy} this site is occupied with a TC with probability $w(t(\mathbf{r},\tau)=0\rightarrow\ t(\mathbf{r},\tau)=1)=\Delta\tau/T_t$ and $c_{GF}(\mathbf{r},\tau)$ is updated. T_t estimates the TC proliferation time, which can vary enormously with different tumors (Hirst et al., 1982).

Vessel growth: (Fig. 1b) Adult normal vessels are quiescent, whereas EC-s in pathologic tumor vessels are stimulated to proliferate and migrate by a local increase in GF concentration to form sprouts (Risau, 1997), migrate and either meet with an other EC forming a tube, or retract (Nehls et al., 1998). In melanoma TC-s also use existing vessels (Paku, 1998) and the high density of anastomosing network (interconnected vascular tubes) arises from an interplay between cooption of old vessels and subsequently induced sprouting (Thompson et al., 1987; Holash et al., 1999b). The latter scenario was applied in our model.

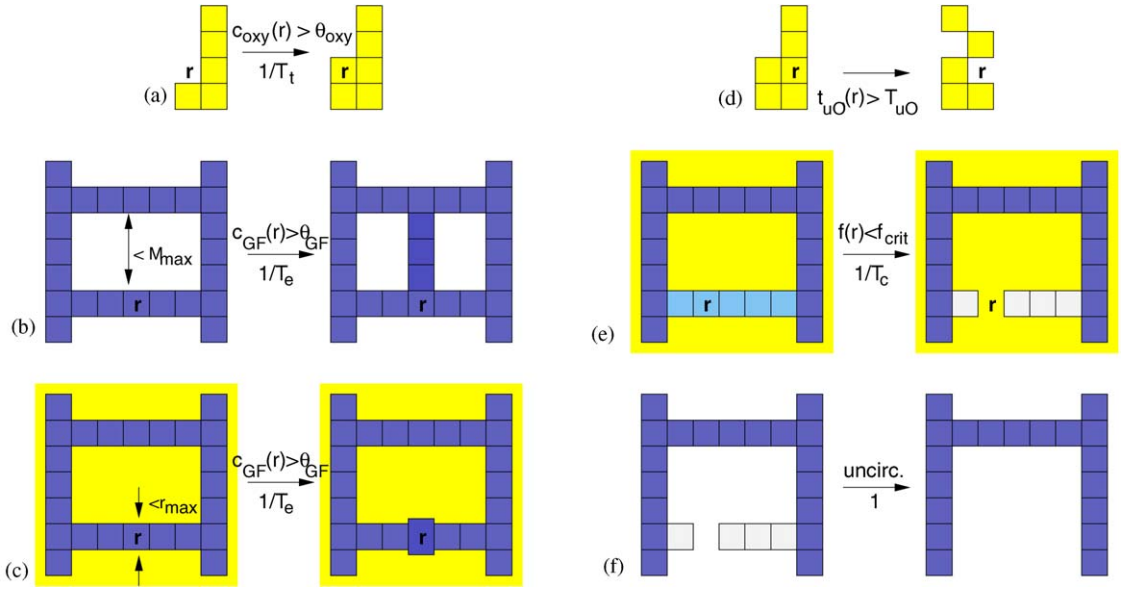

Fig 1. Sketch of the dynamical processes in the model. Yellow boxes represent individual TCs (of lateral size $\Delta r = 10\,\mu m$), blue boxes represent tubular vessel segments of length $\Delta r = 10\,\mu m$ and diameter e_r, which is initially also $\Delta r = 10\,\mu m$. Note that several vessel segments build one vessel running between two branching points of the network. Light blue boxes represent weakly perfused vessel segments with low shear force e_f, white boxes represent non-circulated vessels. (a) *TC proliferation* at a tumor surface site **r** occurs with a rate $1/T_t$ if the O_2-concentration c_{oxy} at **r** is larger than the threshold θ_{oxy}. (b) *Vessel growth* from a starting site **r** occurs with a rate $1/T_e$ if the GF-concentration c_{GF} at **r** is larger than the threshold θ_{GF} and the distance to the next level is smaller than the maximum sprouting distance M_{max}. The new vessel must not touch other vessels except at the start and end-point. (c) *Vessel dilatation*: vessel segments at site **r** inside the tumor (indicated by the yellow back-ground) with a radius $e_r(\mathbf{r})$ less than r_{max} increase their radius with a rate $1/T_e$ if the GF-concentration c_{GF} at **r** is larger than the threshold θ_{GF}. The increase of the radius $e_r(\mathbf{r})$ is indicated by an increase of the cross-section of the corresponding box: vessel connecting two junctions in the network can have segments with varying radius. (d) *TC death*: if a TC at site **r** was longer than the time T_{uO} in an under-oxygenated state, it is removed. (e) *Vessel collapse*: if the shear force f inside a vessel at site **r** inside the tumor (indicated by the yellow background) is smaller than f_{crit} it collapses with a rate $1/T_c$. Such a collapse event can leave other vessel segments un-circulated, as indicated. (f) *Vessel regression*: un-circulated vessels are removed (with probability 1).

New straight vessel segments between two circulated vessels at site **r** and **r′** are introduced with probability $\Delta\tau/T_e$ (where T_e is the estimated EC proliferation time) if: $c_{GF}(\mathbf{r},\tau) > \theta_{GF}$, no site in the migration path is occupied by TCs, no site and no neighbor site of the migration path is occupied by ECs except **r** and **r′**, and $|\mathbf{r}-\mathbf{r}'| < M_{max}$. (The latter condition incorporates the experimental observation (Nehls et al., 1998) that sprouts migrate only a maximum distance and retract if they do not meet another vessel their path, thus not forming a new vessel. M_{max} therefore has the meaning of a maximum sprout migration distance.) In case of such an event $e(\mathbf{r},\tau) = 1$ and $e_r(\mathbf{r},\tau) = r_0$ along this path, and $S_{circ}(\tau)$ and $c_{oxy}(\mathbf{r},\tau)$ are updated.

Vessel dilation: (Fig. 1c) Vessel diameter increases in response to GF, vasodilation is reported to occur concomitantly with capillary growth (Carmeliet and Jain, 2000). Vessel perimeters were found to be increased inside the tumor, in the tumor center EC-s were suggested to participate in vessel dilation (Döme et al., 2002).

In our model a vessel segments at site **r** that is surrounded by TCs and has a GF concentration $c_{GF}(\mathbf{r},\tau)$ larger than θ_{GF} increase its radius $e_r(\mathbf{r},\tau)$ by an amount $r_0/2\pi$ with probability $\Delta\tau/T_e$ as long as $e_r \leqslant r_{max}$, the maximum vessel radius. Note that $r_0/2\pi$ corresponds to the amount by which a cylindrical vessel segment increases if a single EC of lateral size r_0 would be inserted into its vessel wall. To mimic the smoothening effect caused by the surface tension of the vessel walls the location of the dilation is shifted to a neighboring vessel segment if a radius difference larger than $r_0/2\pi$ would arise at the original location.

Vessel collapse: (Fig. 1e) Focal necrosis is commonly observed in solid tumors in regions, where the vascular network is inadequate (Griffon-Etienne et al., 1999; Ramanujan et al., 2000). Reduced perfusion of these vessels can be the result of a solid stress of neighboring tumor cells causing the collapse of vessels, or due to apoptosis of ECs induced by local inhibitors of angiogenesis (Dimmeler and Zeiher, 2000). Long-term reduction of wall shear stress is associated with dramatic reduction of the vessel diameter, up to complete vessel occlusion. We used both criteria to identify critical vessels: circulated vessels, which are surrounded by TCs, collapse with probability $p = \Delta\tau/T_{collapse}$ if the wall shear stress $e_f(\mathbf{r},\tau)$ is below a critical value f_{crit}, c.f. Fig. 2b–d. After each collapse event $e(\mathbf{r},\tau) \to 0$ first the set of circulated sites $S_{circ}(\tau)$ and then $c_{oxy}(\mathbf{r},\tau)$ is updated.

Vessel regression: (Fig. 1f) Vessel network sites **r** that are not circulated and under-oxygenated ($c_{oxy}(\mathbf{r},\tau) < \theta_{oxy,EC}$) are eliminated with probability ½. $\theta_{oxy,EC}$ is set 10 times

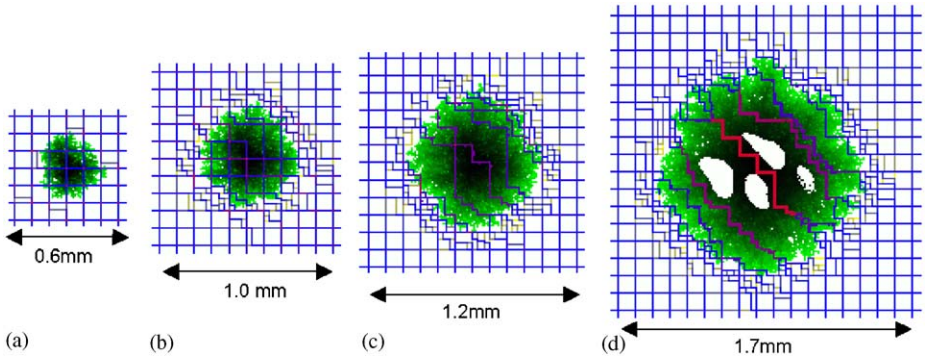

Fig. 2. (a–d) Series of images showing the time evolution of the tumor and vessel configurations in our model at different time steps. The normal vasculature, to be seen far away from the tumor, is characterized by straight lines arranged in a grid like network with a characteristic line-to-line distance (here 100 μm) defining the normal MVD (here 100/mm^2). The color of the blood vessels indicate their blood flow. Blue corresponds to normal, red to high and yellow to low flow values. The thickness of the lines represents the vessel radius. Sites occupied by TCs are color coded in green to black, increasing darkness indicating their age. White regions are empty sites, i.e. inside the tumor the necrotic regions. For the parameter values see the text and Table 2. Only the part of the whole system ($L = 512$) containing the peritumoral region is shown. (a) One time step ($t = 1$) after the initialization of the system: the irregular structure of the initial tumor is typical for an Eden cluster (Eden, 1961). One sees that five new vessels are formed within one time step at the boundary. (b) $t = 50$: extensive formation of new vessels can be seen at the peritumoral region. New vessels frequently have lower blood flow values than vessels in the original network. The original vessels are almost all intact. (c) $t = 100$: the progressive tumor growth pushes the peritumoral plexus further into the normal tissue. Inside the tumor, MVD is drastically reduced leaving large regions of the tumor underoxygenated. (d) $t = 200$: TCs inside the low MVD region visible in (c) died after being 100 times steps in an underoxygenatd state leaving a large necrotic region to be seen a white spots.

higher than the corresponding threshold for TCs, see below.

TC death: (Fig. 1d) TCs adapt their metabolism to hypoxic conditions, therefore $\theta_{oxy,TC}$ is set 10 times lower as $\theta_{oxy,EC}$. TC lifespan under hypoxia and normoxia is difficult to estimate because hypoxia was found to induce apoptosis of TCs but simultaneously lead to selection of p53 deficient colonies induced in hypoxic regions (Yu et al., 2002).

In our model a TC is eliminated with probability ½ only if O_2 concentration is under the low (adapted) $\theta_{oxy,TC}$ for a time T_{uO}. After elimination $c_{GF}(\mathbf{r},\tau)$ is updated.

3. Results

3.1. Base case scenario

A scenario is chosen to describe a melanoma type tumor, characterized by an inter-capillary distace of the original vessel network of $a = 100\,\mu m$, a small GF threshold ($\theta_{GF} = 0.01$), a large GF activation radius ($R_{GF} = 200\,\mu m$), a small O_2 threshold ($\theta_{oxy} = 0.05$), a small O_2 diffusion radius ($R_{oxy} = 100\,\mu m$), relatively high vessel collapse probability ($T^{-1}{}_{collapse} = 0.1\,h^{-1}$ and $f_{crit} = 0.5 f_0$). We set TC proliferation time T_t to 10 h, EC proliferation time T_e to 40 h, initial vessel radius r_0 to 10 μm, the maximum vessel radius r_{max} to 35 μm and the maximum sprouting distance to 100 μm, the initial tumor size to TC_0 to 10^3 and the survival time T_{uO} to 100 h. The unit of time $\Delta\tau$ needs to be smaller than the fastest process in the model, which is TC proliferation: $\Delta\tau = 1\,h$ turns out to be sufficiently small, we checked that decreasing it further leaves our results unaffected.

The inter-capillary distance a of the original network is chosen to reproduce the MVD of normal skin tissue: experimentally the MVD is measured by cutting tissue slices and counting the vessels that cross this slice and these two-dimensional slices are taken from a three-dimensional sample and gives an MVD_0 of ca.100 vessels per mm^2 (Döme et al., 2002), which gives an average capillary distance of $a = 100\,\mu m$. We adopted this distance also for our two-dimensional model, for which one obtains then an average oxygen concentration of $c_{oxy} = 0.2$.

The value for R_{GF} was motivated by the size of the peritumoral region with increased MVD around melanoma measured in (Döme et al., 2002). A small value for θ_{GF} makes sure that indeed new vessels can be formed in this region. The value for R_{oxy} is taken from the experimental data reviewed in (Carmeliet and Jain, 2000). A small value for θ_{oxy} is chosen because increased cellular proliferation in tumors results in a switch from O_2 consuming to glycolytic pathways providing TCs with an alternative energy source during low O_2 supply (Iyer et al., 1998; Minchenko et al., 2002). As already mentioned above, the estimates for the TC proliferation time T_t can vary enormously with different tumors (Hirst et al., 1982), $T_t = 10\,h$ is not unreasonable, and we assume ECs to proliferate four times slower. Parameter values for collapse probability and critical shear force are taken more or less deliberately ($f_{crit} = 0.5$ means that vessel become unstable once the shear force becomes less than ½ of that in normal capillaries). As results do not depend critically on these choices quantitative dependencies are discussed later.

The initial and maximum vessel radii, r_0 and r_{max}, are set to 10 and 35 μm, respectively, motivated by experimental data for melanoma (Döme et al., 2002). The maximum sprouting distance r_{max} is assumed to be 100 μm since

sprouting occurs mainly in the peritumoral region where the intercapillary distance is less than 100 μm. The time T_{uO} that TCs can survive in an underoxygenated state is deliberately set to 100 h, it defines the time lag between removal of one or more vessels and the death of TCs depending on these vessels. The initial tumor size is chosen to be large enough to produce a peritumoral region with sufficiently large GF concentration.

Fig. 2 demonstrates the time evolution of the tumor and vessel configuration in the model with the set of parameter values above (see also Table 2). At late stages of the emergence a phenomenological compartmentalization becomes transparent, see Fig. 3: (1) The outer region close to the tumor surface (peritumoral tissue) is highly vascularized by thin vessels, its thickness depends on θ_{GF} and R_{GF}; (2) a well circulated tumor region (tumor periphery) containing vessels grown via sprouting in the outer shell and then enclosed by the growing tumor; (3) the intermediate region inside the tumor with lower MVD and thicker vessels; and (4) the necrotic core with only a few large and stable vessels enclosed by a cuff of TCs, the thickness of which depends on θ_{oxy} and R_{oxy}. The border between regions 2 and 3 is diffuse.

A quantitative analysis of this time evolution is performed as follows: at each time MVD, O_2 and GF concentration, vessel radius, shear stress, blood flow and pressure inside the vessels are calculated as a function of the radial distance r from the tumor center. Results for the tumor density and MVD is shown in Fig. 4. The peak in the height profile of the tumor density indicates the boundary of the tumor (stochastic fluctuations in the TC

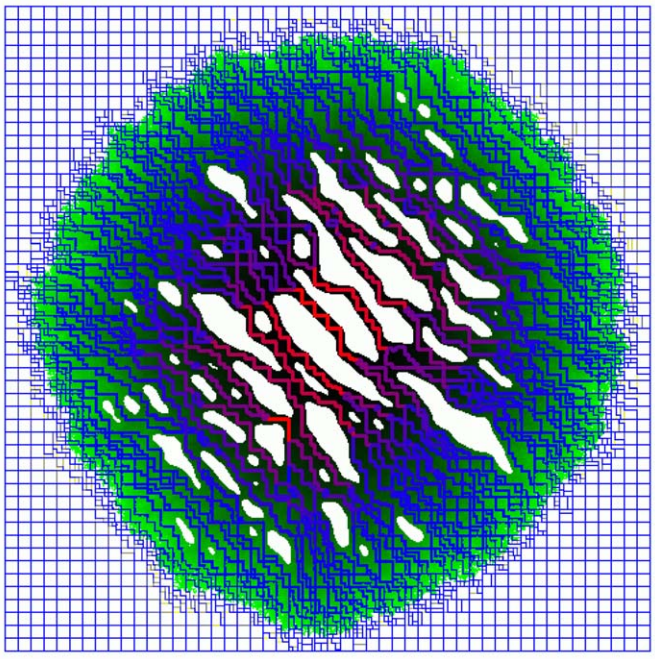

Fig. 3. The state of the system with the same parameters as in Fig. 1 after $t = 1000$ time steps. The color coding is the same as in Fig. 2. The lateral size of the region shown is 5.1 mm.

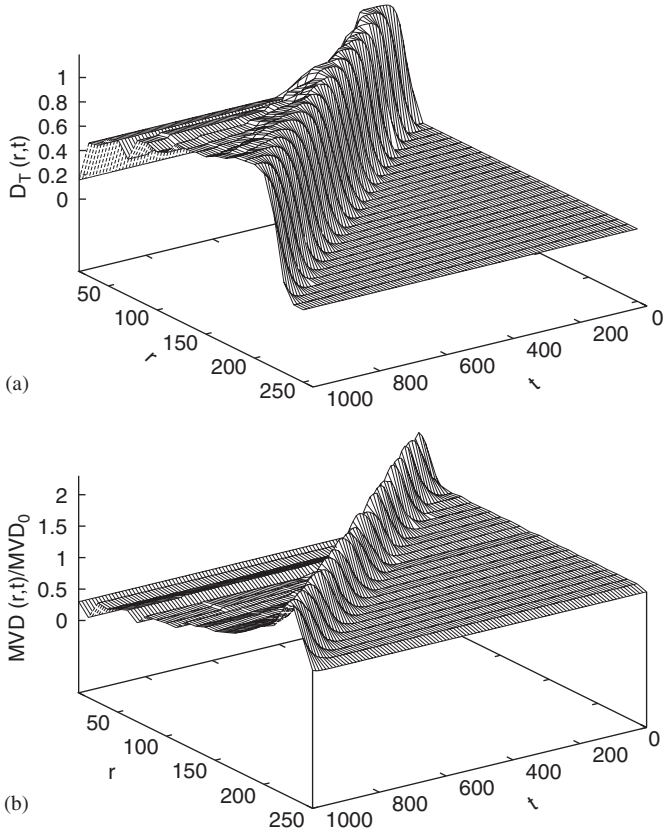

Fig. 4. As a function of the radial distance r from the tumor center (measured in units of Δr) and the time t (measured in units of Δt) it is shown: (a) the average tumor density $D_T(r,t)$ as defined by the average number of TCs per lattice sites at time t, (b) average microvascular density MVD(r,t), the average number of vessels per lattice site, relative to normal tissue MVD_0. The average is done over an annulus of width $10\Delta r$ with central radius r.

proliferation as well as inhomogeneities in the O_2 concentration cause the finite width of this step). The tumor radius $R_{tumor}(\tau) = \max\{r|D(r,\tau) = 1/2\}$, also shown in Fig. 4a, grows linearly with time, a fit yields $R_{tumor}(\tau) = 0.21\tau + 30$ (time and radius measured in units of $\Delta\tau$ and Δr, respectively). The radial growth rate (0.21) is approximately twice the TC proliferation rate ($\Delta\tau/T_t = 0.1$), which is typical for Eden growth. As long as the peritumoral vessel plexus develops fast enough (small $\theta_{oxy,EC}$, large R_{GF}) $R_{tumor}(\tau)$ displays the same time dependence.

At the peak D_T develops a plateau of width $\sim 50\Delta r$ before it decreases substantially due to the appearance of necrotic regions in the tumor center. The irregularities in the density profile reflect the exact spatial locations of these necrotic regions, which is random. An average over several realizations of the stochastic process that is described by our model would remove these fluctuations and yield smooth curves. This remark holds for all Figs. 3 and 4.

The average growth factor concentration $c_{GF}(r,\tau)$ has approximately the same shape as the tumor density, which is due to the fact that all viable TCs contribute to $c_{GF}(r,\tau)$ in the same way (data not shown).

Fig. 4b shows the MVD, which has a sharp maximum at a radius $R_{MVD}(\tau)$, corresponding to a highly vascularized tumor periphery, which evolves also linearly with time. A fit yields $R_{MVD}(\tau) = 0.21\tau + 30$, implying that it is identical with the tumor radius $R_{tumor}(\tau)$ and demonstrating the appearance of a highly vascularized region in the peritumoral tissue. For radii $r < R_{MVD}(\tau)$ the MVD drops quickly (within ca. $50\Delta r$) to values around the normal tissue MVD_0 before slowly decreasing to values significantly lower than MVD_0 (corresponding to a poorly vascularized tumor center). In (Döme et al., 2002) the morphometry of human malignant melanoma (hMM) was analysed and data for MVD and vessel perimeter were obtain in three different regions of the tumors: (I) the tumor center, (II) the tumor periphery—a 100 μm wide band of tumor immediately adjacent to the invasive edge; and (III) the peritumoral host tissue—a 200 μm wide band of host connective tissue immediately adjacent to the tumor periphery. It was found that for melanoma larger than 1.5 mm the MVD at the tumor centre was ca. 50% of the normal tissue MVD_0, at the tumor periphery it was ca. 50% more than MVD_0,and at the tumor perimeter it was ca. two times MVD_0. These data are in good agreement with ours.

The O_2 concentration profile $c_{oxy}(r,\tau)$ (not shown) has approximately the same shape as $MVD(r,\tau)$ reflecting the fact that all vessel segments contribute in the same way to $c_{oxy}(r,\tau)$. Hypoxic conditions in the tumor center can thus directly be read off from the MVD.

The average vessel radius is found to grow linearly with time inside the tumor, as can be seen in Fig. 5a. The maximum vessel radius, set to $r_{\max} = 3.5\Delta r$, appears as a plateau at sufficiently large times. This behavior is characteristic for a situation in which the GF concentration $c_{GF}(\mathbf{r},\tau)$ inside the tumor ($r < R_{tumor}(\tau)$) is always larger than the actual GF-threshold (θ_{GF}). Comparing again our results fro the vessel radius in the three tumor regions (center, periphery and perimeter) with the experimental data for melanoma (Döme et al., 2002) one observes a good agreement.

The average blood flow per vessel, shown in Fig. 5b, increases proportionally to $(R_{tumor}(t)-r)^4$ towards the tumor center, due to the fact that the flow depends on the 4th power of the vessel radius, which increases linearly according to Fig. 5a. Finer variations of the flow in the peritumoral region are present but not visible on the chosen scale, but see Fig. 5c.

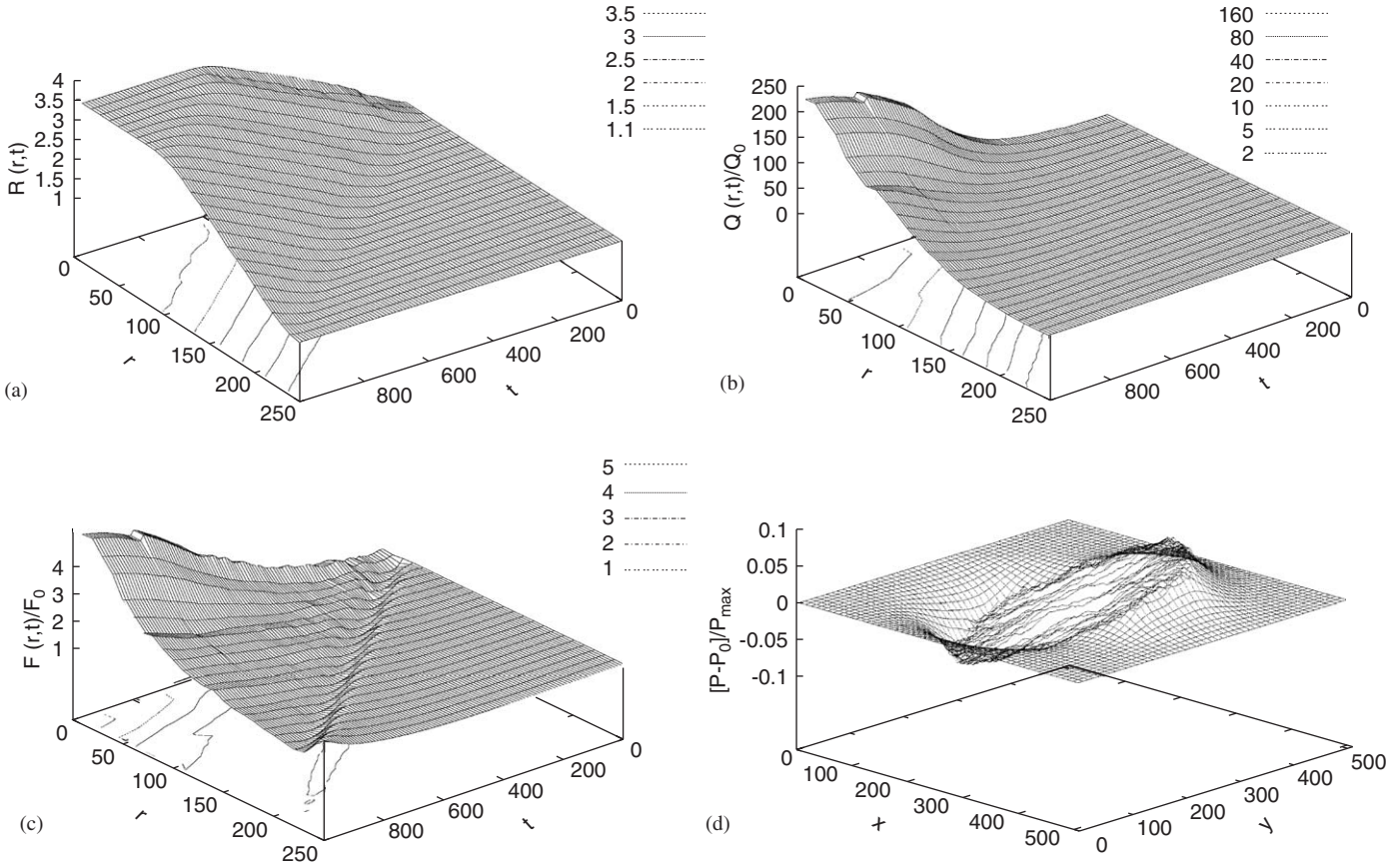

Fig. 5. As in Fig. 4 it is shown as a function of the radial distance r from the tumor center and the time t: (a) the average vessel radius $R(r,t)$, (b) the blood flow per vessel $Q(r,t) = e_q(r,t)$, (c) the shear stress $F(r,t) = e_f(r,t)$. (d) The difference in the blood pressure inside the vessels (with respect to normal). Since the local blood pressure inside the vessels does not have the radial symmetry of the other quantities studied in a–c we show the pressure field $P(x,y)$ at time $t = 600$ minus the normal pressure $P_0(x,y)$ at $t = 0$ (i.e. for normal vascularization), where (x,y) are the coordinates of the vessels. One recognizes the spatial location and extent of the circular tumor in the middle. The global flow direction, enforced via the boundary conditions, is from left (0,0) to right (512,512). Looking along this direction, the pressure is decreased in front of the tumor (left) and increased at the back of the tumor (right).

The shear stress $F(r,t)$ acting upon the vessel walls is shown in Fig. 5c. It displays a pronounced dip where the MVD (Fig. 4b) has its maximum, i.e. in the peritumoral plexus. This is due to the fact that an increased MVD in some region reduces the average blood flow per vessel and concomitantly the shear stress F. According to the definition of the model vessels with $F<F_{crit}$ ($=0.5F_0$ here) can collapse resulting in MVD decrease, flow increase and shear stress increase–which is visible in Fig. 5c towards the tumor center (see Fig. 6).

Fig. 5d shows the difference between the blood pressure in the vessel at location (x,y) in the normal vasculature and the blood pressure in the tumor vasculature at time $t=600$, normalized to the maximum pressure in the upper left corner ($x=0, y=0$). The blood pressure gradient in the tumor center is up to 50% lower than in normal vessels in spite of the decreased MVD. This is due to dilated vessels with a blood flow capacity up to 200 times larger than that of normal vessels (Fig. 5b).

We determined the fractal dimension d_f of the vascular network with the box-counting method (Mandelbrot, 1983) with boxes ranging from lateral size $1\Delta r$ to $100\Delta r$, the result is shown in Fig. 6, and find it to depend on the tumor region to which the analysis was restricted. The original vasculature has $d_f=2.0$ per construction since the Manhattan pattern represents a compact structure. The complete vasculature that was altered by the tumor has $d_f=1.85\pm0.05$, concurring with the estimate for the capillary network of various carcinoma $d_f^{carc}=1.89\pm0.04$ (Gazit et al., 1995), and also with the exactly known value for conventional percolation $d_f^{perc}=1.891$ (Stauffer and Aharony, 1992). The restriction of the analysis to concentric annular rings of width $50\Delta r$ yields a value of $d_f=1.60\pm0.05$ for the peritumoral region and slightly decreasing values for decreasing radii of the rings reflecting the increasing sparseness of the vessels towards the tumor center. All measurements of fractal aspects of tumor vasculature suffer from the fact that the possible box-sizes span only 2 decades (in real tumors as well as in our model): the minimum size is ca. 10 μm (approximately the minimum diameter of a capillary) and the maximum is around 1 mm (for a tumor of size 5–10 mm). Taking into account error bars and transient regimes it is clear that a precise estimate of d_f is hardly feasible. Differences in d_f of the order of 0.1 are, however, significant, and indicate that the local values for d_f correlate strongly with local values for the MVD.

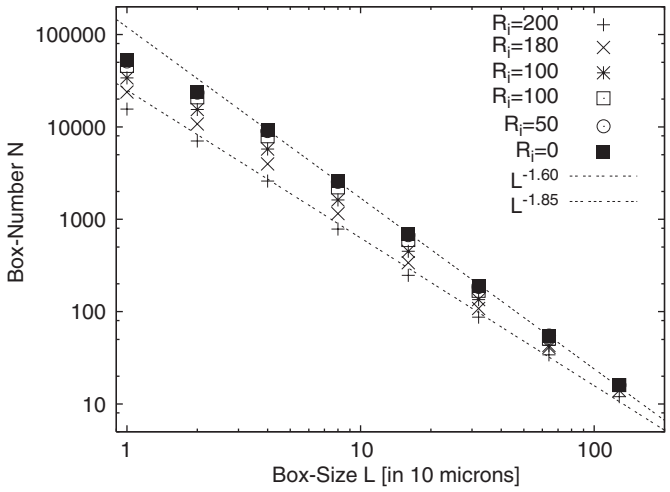

Fig. 6. Determination of the fractal dimension d_f of the vessel network at time t in the base case (Fig. 2) via the box-counting method: the number of Boxes of size L that is needed to cover completely the vasculature is plotted as a function of L in log–log scale. The slope d_f of the curve is the fractal dimension. We confined the measurement to annuli with fixed outer radius that is determined by the limit of the peritumoral plexus and with varying inner radius R_i. The slope of the curves decreases with increasing R_i: $d_f=1.85\pm0.05$ for $R_i=0$ (full squares, which corresponds to the complete tumor vasculature) and $d_f=1.60\pm0.05$ for $R_i=200$ (which corresponds to the peritumoral plexus exclusively), indicating that the fractal dimension is not a homogeneous measure over all regions of the tumor vasculature.

3.2. Parameter dependencies

In the following we analyse the various parameter dependencies of the model. Since tumor growth in our model depends strictly on the concentration field $c_{oxy}(\mathbf{r})$ it is useful to clarify the shape of this field in the original vasculature, which is shown in Fig. 7 for different values of the lattice constant of the original vasculature a (i.e. different values of the original $\mathrm{MVD}_0=1/a^2$). The oxygen concentration in the original tissue varies spatially only within a few percent when $R_{oxy}\geqslant a$ and its mean value c^0_{oxy} is proportional to MVD_0. TCs at the tumor surface will always survive and proliferate when $\theta_{oxy}<c^0_{oxy}$. On the other hand when $\theta_{oxy}>c^0_{oxy}$ or when R_{oxy} is smaller than a the regions between two neighboring vessels in the original network have a O_2 content much lower than c^0_{oxy} (or even zero if $R_{oxy}<a/2$), the survival and eventual growth of the tumor becomes probabilistic and depends upon the speed with which new vessels are formed—survival probability

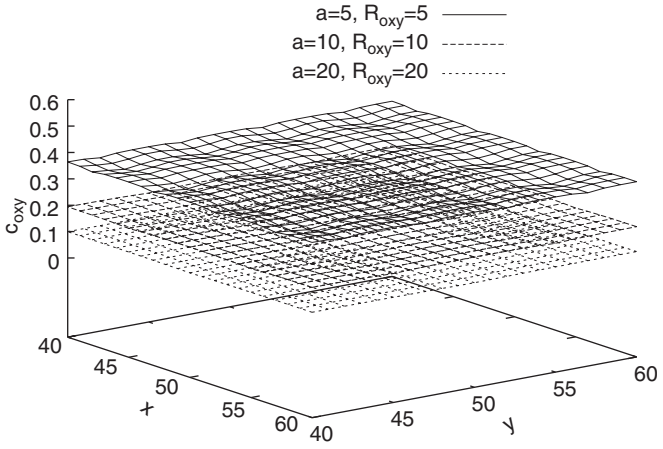

Fig. 7. Oxygen concentration field $c_{oxy}(x,y)$ of the original vasculature for different lattice constants a ($a=5$, 10, and 20 Δr), i.e. different MVD_0. R_{oxy}, is here chosen to be equal to a. The variation of c_{oxy} between the vessels is only a few percent and the average value decreases with decreasing a (or MVD_0).

decreases drastically in this parameter region and the tumor morphology can become non-circular and even disconnected. In later stages of the tumor growth R_{oxy} and θ_{oxy} determine the diameter of the cuffs surrounding the large vessels inside the necrotic regions of the tumor.

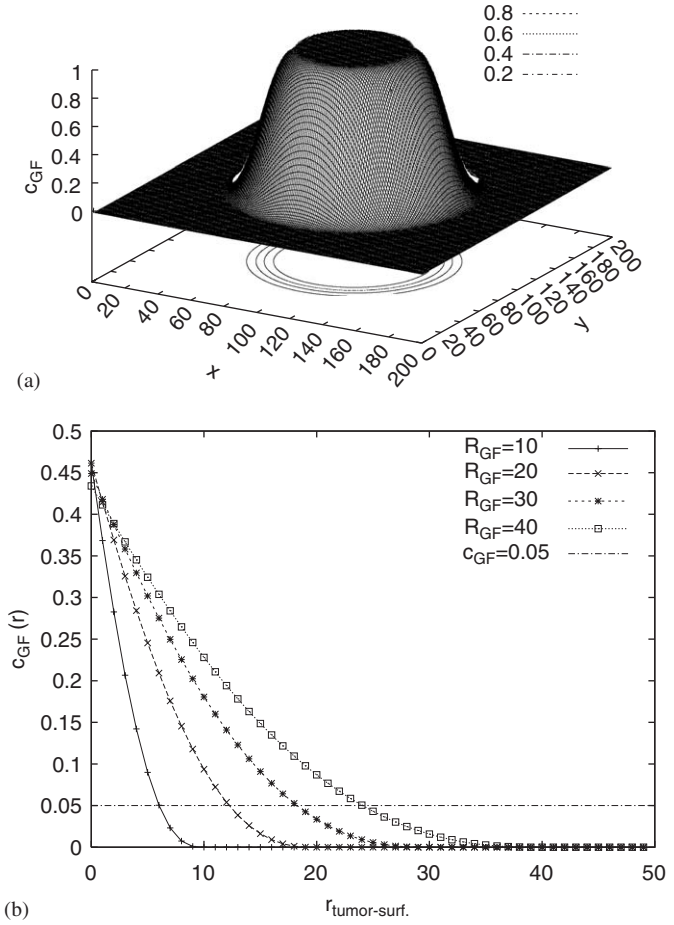

Fig. 8. (a) (Top) Growth factor concentration field $c_{GF}(x,y)$ for an ideal circular tumor of density one and radius $50\Delta r$ and $R_{GF} = 20\Delta r$. (b) (Bottom) c_{GF} as a function of the distance from the tumor surface for the ideal tumor with different R_{GF}.

To clarify the effect of R_{GF} and θ_{GF} we show the GF concentration field $c_{GF}(\mathbf{r})$ produced by an ideal circular tumor with density 1 and radius $50\Delta r$ in Fig. 8a. In the tumor center $c_{GF}(\mathbf{r}) = 1$ due to the normalization of the function $f_{GF}(r)$. At the boundary the concentration profile decreases in a sigmoidal shape from 1 to 0 over a width of $2R_{GF}$, being 0.5 approximately at the tumor surface. In Fig. 8b we show c_{GF} as a function of the distance r from the tumor surface for different values of R_{GF}. c_{GF} scales linearly with R_{GF} which implies that the limit of EC growth, i.e. the width of the region outside the tumor with increased MVD, increases linearly with R_{GF}, as is illustrated by the straight line at $c_{GF} = 0.05$, from which the maximum width of this region can be read off for the case θ_{GF}.

A non-trivial consequence of large values of R_{GF} (e.g. $40\Delta r$), which produce a wide and dense vasculature in the peritumoral region, is that they are accompanied by larger MVDs also inside the tumor thus inhibiting the emergence of necrotic regions for a large range of collapse probabilities and critical flows—Fig. 9a shows an example of a Monte-Carlo simulation for $R_{GF} = 40\Delta r$ and all other parameters as in the base case.

The collapse probability $p_{collapse} = \Delta\tau/T_{collapse}$ and the critical shear stress f_{crit} determine the total necrotic volume and the total vessel number, as is demonstrated by the examples shown in Figs. 9b and 10. In Fig. 9b all parameters are the same as in Fig. 9a, only f_{crit} is changed from 0.5 to 0.7, which means that higher flow values are necessary to stabilize vessel. This moderate change decreases MVD inside the tumor drastically and produces large necrotic regions. In Fig. 10 a series of configurations with increasing collapse probability $p_{collapse}$ is shown. The necrotic volume relative to the total tumor mass as well as to the total number of vessels as a function of time for

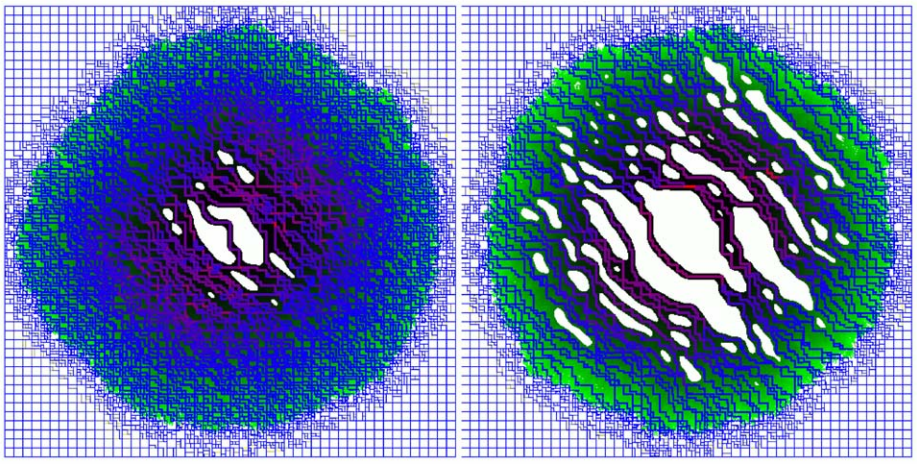

Fig. 9. Effect of a large value of R_{GF} on the tumor morphology. *Left*: shows a configuration after 1000 time steps for $R_{GF} = 40\Delta r$ but all other parameters as in the base case. Compared to Fig. 3 the necrotic regions are much smaller and the MVD is homogeneously increased with the tumor. *Right*: parameters as in the left figure except the critical shear stress f_{crit}, which is now 0.7 (instead of 0.5). Whereas the morphology in the left figure is rather stable even for large collapse probabilities only a small variation of f_{crit} produces large necrotic regions and decreased MVD within the tumor.

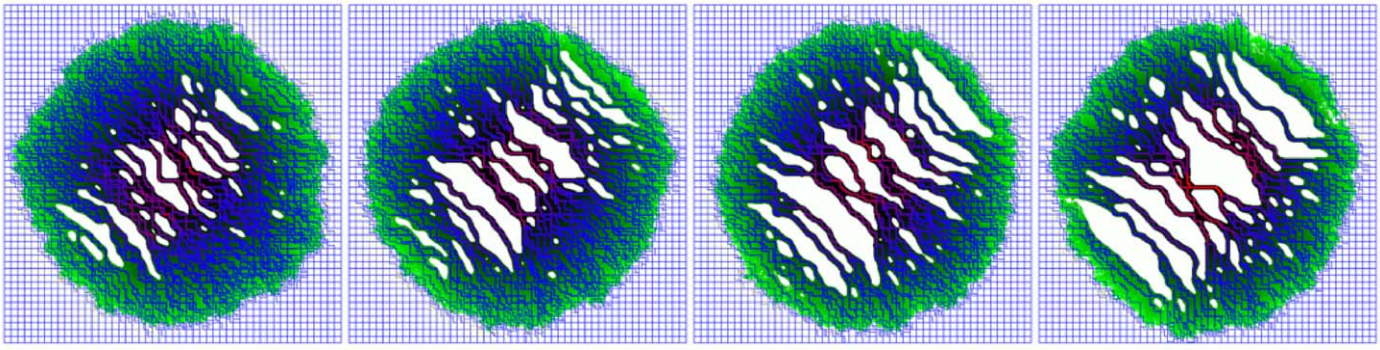

Fig. 10. Sequence of configurations with increasing collapse probability (from left to right it is $p_{collapse} = 0.02, 0.04, 0.1, 0.5$) and $f_{crit} = 0.5$. Here we have chosen $R_{GF} = 10$, $\theta_{GF} = 0.01$ and the other parameters as in the base case. The same seed for the random number generator for the simulations in all cases is chosen to emphasize the effect of the variation of $p_{collapse}$.

different collapse probabilities is shown in Fig. 11 ($f_{crit} = 0.5$ and the other parameters as in the base case). The necrotic volume relative to the tumor mass starts to increase with time for $t > t_{uO}$ and saturates around $t = 500$, ranging from 0.2 for $p_{collapse} = 0.05$ to 0.35 for $p_{collapse} = 0.5$. This means that the tumor has reached a more or less stationary state in which a constant fraction of the tumor mass is necrotic, except for very small values of $p_{collapse}$, where the necrotic regions are confined to a small region at the tumor center: the data for $p_{collapse} = 0.015$ show a slow decrease in the relative necrotic regions for $t > 500$. The total number of vessels at time t decreases linearly with time for $p_{collapse} > 0.05$, and decreases with increasing $p_{collapse}$. For instance for $p_{collapse} = 0.5$ (and again the other parameters as in the base cae) the total vessel number in the system is 25% less than the total vessel number in the original tissue (in the space region considered) after $t = 1000$ time steps although the MVD is substantially increased in the peritumoral region. Only for small values of $p_{collapse}$ the MVD increases for $t > 500$, concomitantly with the decrease in relative necrotic volume: since vessel collapse is rare the increased MVD in the peritumoral region also survives inside the tumor.

The TC proliferation time T_t determines the tumor growth speed in well oxygenated regions. The EC proliferation time T_e determines the speed with which new vessels are formed in regions with sufficient GF and therefore also effects the tumor growth speed if θ_{oxy} is smaller than the critical value (0.12 for $\mathrm{MVD}_0 = 100/\mathrm{mm}^2$).

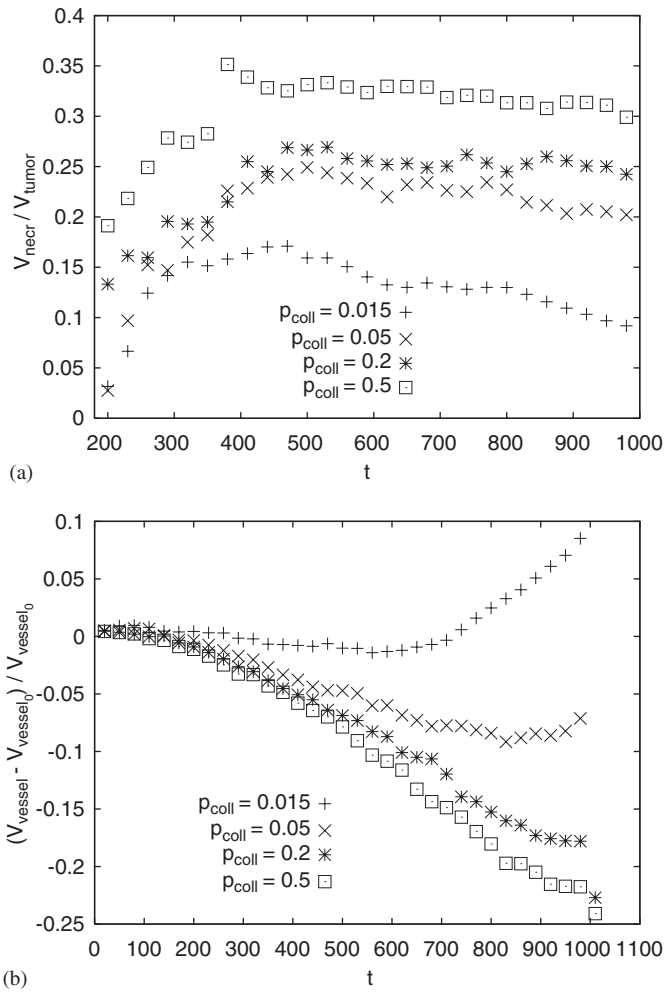

Fig. 11. (a) The total volume of the necrotic regions with the tumor divided by the total tumor mass as a function of time for different collapse probabilities (parameters as in Fig. 9). (b) The relative deficit/excess volume of the vasculature as a function of time for different collapse probabilities (parameters as in Fig. 9).

4. Discussion

Within the base case scenario we have demonstrated that the model describes phenomenologically very well the spatially resolved experimental data of Döme et al. (2002) for vessel radii and MVD in melanoma. The model can also be adopted to other tumor growth scenarios, ranging from tumors with a low oxygen demand that exclusively coopt pre-existing vessels to tumors that produce a characteristic peritumoral vascular plexus because of high oxygen demand or high GF production rate. It also describes scenarios in which tumors are completely filled

with viable TCs and high MVD in the center on one side and morphologies containing large necrotic regions and only a few very thick vessels on the other side.

An important prediction of our model is that large parts of the vascular network can be cut off from the blood circulation by the collapse of only a few vessel segments, namely those which are located in the perimeter of this part of the network. Consequently the emergence of necrotic regions does not necessarily rely on the presence of large amounts of anti-angiogenic factors (Ramanujan et al., 2000). We find that failure of only a few vital ECs induced by the local mechanical pressure of high tumor densities might also be sufficient to disrupt the oxygen supply of a whole region leading to massive cell death therein. The vessel segments need not only to be connected to the exterior network via an uninterrupted path but at least bi-connected (equivalent to the existence of at least two link-disjoint, uninterrupted paths) in order to be circulated by the blood flow, which lowers the number of collapses that would lead to the necrosis of a region even further.

Vessel collapse events have been shown to correlate with elevated levels of solid pressure exerted by the growing tumor on the intratumoral vessel wall (Boucher and Jain, 1992), which is considered qualitatively in the present version of our model by the criterion that collapse events only occur, if the vessel is surrounded by TCs. Varying stiffness of the surrounded matrix in different tumors can phenomenological be described in our model by varying values for the collapse probability.

In addition to the criterion that vessels are surrounded by TC-s, shear stress was chosen as a second parameter to correlate collapse events. This was motivated by the data obtained on normal vessels, where temporal changes in the hemodynamic flow pattern causing locally a decrease in wall shear stress were shown to lead to a structural reduction of the internal vessel diameter (Pries et al., 1995). We suggest therefore that for a vessel which is surrounded by TC-s (also exerting solid stress) such a contraction could lead to complete collapse.

Another important prediction is that vessel collapse and the local blood flow characteristics have to be correlated via the local shear stress. If the collapse events would occur independent from one another with some probability p, a fundamental law in percolation theory (Stauffer and Ahorony, 1992) predicts that either the interior of the tumor is completely filled (i.e. does not contain large connected necrotic regions) or it is completely void up to a small boundary region—except for one special value for the parameter p, the percolation threshold p_c. We confirmed this scenario by testing different model variants containing uncorrelated collapse events (see Appendix and Fig. 12). The existence of a model parameter like the collapse probability that has to be fine-tuned to a special value in order to reproduce vessels that thread the whole tumor would obviously be unsatisfactory. Only if we correlated the vessel collapse with the shear stress the model predicts a realistic vascular network morphology that is robust against parameter variations. The basic mechanism for this robustness is the redirection of the flow after collapse events into still intact vessels resulting in an increased shear stress in the remaining vessels and thus a drastically reduced collapse probability. Shear stress rather than blood flow as a hemodynamic criterion for vessel stability appears to be plausible, since the ECs in the vessel wall have informations about the shear stress but probably less about the total flow. We checked that a correlation of vessel collapses with the blood flow also leads to unrealistic network morphologies in which only a few vessels survive within the whole tumor (i.e. a tumor periphery with increased MVD is completely missing). The reason for this is the dependence of the flow from the fourth power of the vessel radius. This leads to a strong variation of the flow between vessels of only slightly different radius implying the survival of only the thickest vessels if collapse is correlated with the flow.

Blood vessels are exposed not only to shear stress but also to the transmural pressure. Since the physiologically relevant difference between the microvascular pressure and interstitial fluid pressure is generally very low in tumor vessels due to their leakiness (Boucher et al., 1996), the pressure-shear hypothesis (Pries et al., 1995) implies an adaptation of the vessel walls towards low equilibrium

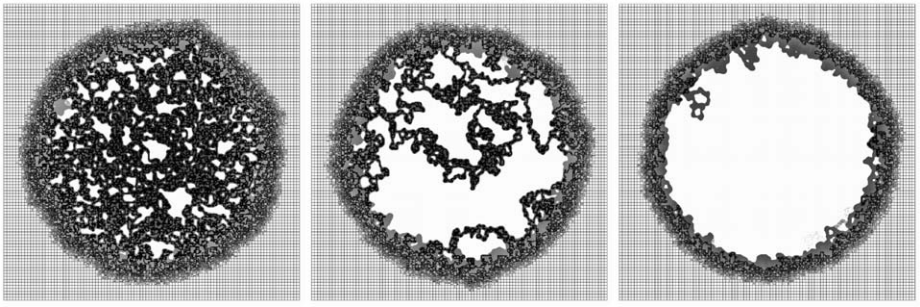

Fig. 12. Tumor and vessel configurations after time $t = 2000$ for the model with uncorrelated vessel collapse (i.e. without blood flow and without a critical shear foce determining the vessel collpase)—from left to right it is $p_{collapse} = 0.04$, 0.05 and 0.06. The morphology of the vessel network is much more tortuous, in particular a global directedness of the vessel is absent and only for values of $p_{collapse}$ around 0.05 the inner region of the tumor is neither completely filled nor completely void with thick vessels threading the tumor.

shear-stress via vasodilation. Together with the effect of GF this mechanism explains the ubiquitous presence of dilated vessels in tumors. Nevertheless blood pressure in tumor vessels remains enigmatic: it is usually larger than the pressure in normal vasculature in spite of the increased MVD and larger vessel diameter in tumors. In addition to geometrical effects also the solid stress exerted by the tumor might play an important role. It appears promising to incorporate solid stress into our model, by using a continuum description for the growing tumor.

The analysis of the parameter dependencies of our model revealed that the morphology of the tumor vasculature depends most strongly on the potential width of the peritumoral plexus (related to the diffusion range of the growth factor molecules) and on the way in which the process of vessel collapse takes place. Varying the probability with which vessels can collapse translates immediately into a variation of the necrotic volume, even more dramatically upon variation of the critical shear force.

A general feature of the remodeling process of the normal vasculature into the tumor vasculature in the model—and we propose this to hold also for in vivo tumors—is that none of the initial characteristics of the original vessel network survives this process: we assumed a original vascular network that consists of capillaries of equal diameter arranged in a regular grid with a given MVD, which guarantees a homogeneous distribution of oxygen and a constant shear stress in all vessels. Once the tumor grows over it, it gets transformed into a compartmentalized network with irregularly arranged dilated vessels and a decreasing MVD from the tumor periphery to the tumor center, resulting in an inhomogeneous oxygen distribution.

Variations in the structural characteristics of the original vascular network will not influence the compartmentalization of the tumor reported here but will certainly have implications for the emerging network morphology and for the absolute values of microvascular pressure. For instance we observe a global directedness of the central vessels in our model, which is a consequence of the boundary conditions for the hydrodynamic pressure that we assumed, which imprints a global net flow in one particular direction through the tumor. The resulting pressure distribution within the whole network has a diagonal gradient, with higher pressures always on the upper left side of the tumor and lower pressure on the lower right side. Natural vascular networks are organized in arterial and venous trees connected by capillary beds, with blood pressure generally decreasing from arteries over arterioles to capillaries and venoules. Their pressure distribution has therefore a structural basis. It would be useful to initialize our model with an original network that is organized in the same way, because then one can also expect to obtain a realistic distribution of the absolute values of the hydrodynamic pressure within tumor vessels. The modulus of the pressure gradient within tumor vessels should, however, remain decreased towards the tumor center, as in the present version of our model.

The fractal analysis of the tumor vasculature predicted by our model showed that for the base case scenario the fractal dimension d_f is around 1.85, which is close to the value found in various carcinoma $d_f^{carc} = 1.89 \pm 0.04$ (Gazit et al., 1995). This value is close to the exactly known value for conventional percolation $d_f^{perc} = 1.891$ (Stauffer and Aharony, 1992), describing a fractal structure that is obtained by randomly removing bonds from a regular two-dimensional network. We therefore propose that the fractal structure of the tumor vasculature is determined by the stochastic vessel collapse inside the tumor and not by vessel growth processes in the peritumoral region. This view contrasts the with the view of (Gazit et al., 1995), where it has been emphasized that their estimate for d_f of carcinoma vasculature corresponds closely to the one for invasion percolation, (which is, however, $d_f^{inv-perc} = 1.81$ (Furuberg et al., 1988)), hence relating the growth of tumor vasculature to the expansion of a network throughout a medium with randomly distributed heterogeneities in strength. Our model does not involve any heterogeneity aspects of an extracellular matrix surrounding a growing tumor, nevertheless the fractal characteristics of the tumor vasculature turns out to be similar to the one of real tumors.

The tumor radius grows always linear with time in the model and depends strictly on the TC proliferation time, which is a consequence of the restriction of TC proliferation to surface sites, provided they are sufficiently oxygenized. Only in the case of low original MVD it depends on the speed with which the peritumoral region expands into the underoxygenated areas via sprouting. The tumor would stop growing if the MVD in some region of the original tissue is substantially smaller than necessary for TC proliferation, depending on θ_{oxy} and R_{oxy}. In the examples we discussed here it grew linearly because we assumed a homogeneous original tissue. Other possible growth limiting factors include growth inhibitors either produced by the TCs or the host tissue, which could be added as new concentration field into our model, and solid stress generated by a growing tumor in a confined space (Helmlinger et al., 1997) also elevating microvascular pressure (Griffon-Etienne et al., 1999). However involvement of solid stress into the model would lead to a mechanism for growth inhibition only in later stages of tumor development, at present the maximum diameter of the tumor we consider was 5 mm. It would certainly be worthwhile to incorporate elastic TCs into our model according to the lines of (Drasdo and Höme, 2005).

A correlation between tumor expansion and a local MVD value is visible in our model only in the case when the original MVD is too low to meet the metabolic demand of the TC-s. In this case tumor growth will occur and sustain only if GF production is sufficient to stimulate sprouting in the peritumoral region (θ_{GF} is small or R_{GF} is large), MVD must be elevated here. In the tumor center the

MVD depends on the vessel collapse probability, thus can be larger or smaller than, or equal to the normal tissue MVD. On the other hand if the original MVD is large, there is no correlation between tumor growth and increased (outside) or decreased (inside) levels of MVD, neither locally nor globally. Based on this general behavior of our model we conclude that MVD even when measured in different regions of the tumor is not a reliable diagnostic tool to predict the growth of a single tumor. The correlation found between central MVD of human melanoma and the outcome of the disease (Döme et al., 2002) is probably due to metastasis formation which we did not consider here.

Finally a remark on the two-dimensionality of the model we have presented here: It is straightforward to extend our model to three space dimensions (Lee et al., 2006), for which we obtain essentially the same behavior for tumor radius, MVD, vessel radius, flow, pressure gradient, etc., not only qualitatively but also to some extend quantitatively. A difference is for instance that there the fractal dimension of the vessel network is the one for conventional percolation in 3d.

Conclusion: On the basis of a theoretical model, tested on experimental data for human melanoma, it was shown that the microvascular environment of the host is the dominant condition for tumor progression, once this is initiated. Microvascular density within the tumor can be drastically decreased due to the instability of tumor vessels without disturbing the growth at the tumor periphery, implying that MVD measurements might be an unreliable diagnostic tool for tumor progression.

Acknowledgments

We thank Balázs Döme, Haymo Kurz and Sándor Paku for their input and discussions. This study was supported by the Hungarian Grant OTKA T-37454.

Appendix

Here we consider a variant of our model in which the process of vessels collapse is uncorrelated with the blood flow pattern on the network.

We change the definition of the model introduced in the main text by canceling the flow computation and introduce a fully stochastic vessel collapse with a probability $p_{collpase}$: circulated vessels, which are surrounded by TCs, collapse with probability $p_{collpase} = \Delta\tau/T_{collapse}$. After each collapse event $e(\mathbf{r},\tau)\to 0$ first the set of circulated sites $S_{circ}(\tau)$ and then $c_{oxy}(\mathbf{r},\tau)$ is updated. Vessels that have a radius that is larger than a certain threshold r_{stab} are supposed to be stable and cannot collapse any more (without any stabilization mechanism all vessels would eventually vanish).

Fig. 12 shows the result of the simulation of this model with for different values for $p_{collpase}$ (and other model parameters as in the base case) and demonstrates that the absence of a correlation between vessel collapse and blood flow leads to unrealistic vessel morphologies and a sharp percolation transition from configurations with small disconnected necrotic regions for small collapse probabilities to configurations consisting only of small annulus of viable tumor cells.

A more detailed analysis (data not shown) reveals a sharp percolation transition takes place at $p_{collapse} = 0.049$ which is in the same universality class as conventional percolation (Stauffer and Aharony, 1992): essentially in this model variant the vessels can collapse only for a fixed time interval—starting at the point when the tumor grows over them and ending at the point when they reach the stabilization radius (note that the radius grows linear in time once vessels are surrounded by TCs). The collapse rate multiplied with this time interval yields the total probability with which a vessel segment is removed. This process leads naturally to a connectivity percolation transition, and much earlier (i.e. for smaller values of $p_{collapse}$) to a bi-connectivity percolation transition.

References

Alarcón, T., Byrne, H.M., Maini, P.K., 2003. A cellular automaton model for tumour growth in inhomogeneous environment. J. Theor. Biol. 225, 257–274.

Anderson, A.R.A., Chaplain, M.A.J., 1998. Continuous and discrete mathematical models of tumor-induced angiogenesis. Bull. Math. Biol. 60, 857–900.

Boucher, Y., Jain, R.K., 1992. Microvascular pressure is the principal driving force for interstitial hypertension in solid tumors—implications for vascular collapse. Cancer Res 52, 5110–5114.

Bartha, K., Rieger, H., 2006. Morphology of tumor vasulature: a theoretical model. In: Proceedings of the ECMTB 2005; Series: Modeling and Simulation in Science, Engineering and Technology, Birkhaeuser, Boston.

Boucher, Y., Leunig, M., Jain, R.K., 1996. Tumor angiogenesis and interstitial hypertension. Cancer Res. 56, 4264–4266.

Brú, A., Albertos, S., Subiza, J.L., García-Asenjo, J.L., Brú, I., 2003. The universal dynamics of tumor growth. Biophys. J. 85, 2948–2961.

Burri, P.H., Hlushchuk, R., Djonov, V., 2004. Intussusceptive angiogenesis: its emergence, its characteristics, and its significance. Dev. Dyn. 231, 474–488.

Carmeliet, P., Jain, R.K., 2000. Angiogenesis in cancer and other diseases. Nature 407, 249–257.

Cullen, J.P., Sayeed, S., Sawai, R.S., Theodorakis, N.G., Cahill, P.A., Sitzmann, J.V., Redmond, E.M., 2002. Pulsatile flow-induced angiogenesis—role of $G(i)$ subunits. Arterioscler. Thromb. Vasc. Biol. 22, 1610–1616.

Davies, P.F., 1995. Flow-mediated endothelial mechanotransduction. Physiol. Rev. 75, 519–560.

Dimmeler, S., Zeiher, A.M., 2000. Endothelial cell apoptosis in angiogenesis and vessel regression. Circ. Res. 87, 434–439.

Döme, B., Paku, S., Somlai, B., Tímár, J., 2002. Vascularization of cutaneous melanoma involves vessel co-option and has clinical significance. J. Path. 197, 355–362.

Drasdo, D., Höme, S., 2005. A single-cell-based model of tumor growth in vitro: monolayers and spheroids. Phys. Biol. 2, 133–147.

Eden, M., 1961. in: Neyman, J. (ed.), Proceedings of the 4th Berkley Symposium Mathematics and Probability, University of California Press, Berkley, pp. 223–240.

Fears, C.Y., Grammer, J.R., Stewart Jr., J.E., Annis, D.S., Mosher, D.F., Bornstein, P., Gladson, C.L., 2005. Low-density lipoprotein receptor-related protein contributes to the antiangiogenic activity of thrombospondin-2 in a murine glioma model. Cancer Res 65, 9338–9346.

Folkman, J., Bach, M., Rowe, J.W., Davidoff, F., Lambert, P., Hirsch, C., Goldberg, A., Hiatt, H.H., Glass, J., Henshaw, E., 1971. Tumor angiogenesis—therapeutic implications. N. Engl. J. Med. 285, 1182–1186.

Fukumura, D., Yuan, F., Monsky, W.L., Chen, Y., Jain, R.K., 1997. Effect of host microenvironment on the microcirculation of human colon adenocarcinoma. Am.J. Pathol. 151, 679–688.

Furuberg, L., Feder, J., Aharony, A., Jossang, T., 1988. Dynamics of invasion percolation. Phys. Rev. Lett. 61, 2117–2120.

Gazit, Y., Berk, D.A., Leunig, M., Baxter, L.T., Jain, R.K., 1995. Scale-invariant behavior and vascular network formation in normal and tumor tissue. Phys. Rev. Lett. 75, 2428–2431.

Goerges, A.L., Nugent, M.A., 2004. pH regulates vascular endothelial growth factor binding to fibronectin—a mechanism for control of extracellular matrix storage and release. J. Biol. Chem. 279, 2307–2315.

Gödde, R., Kurz, H., 2001. Structural and biophysical simulation of angiogenesis and vascular remodelling. Dev. Dyn. 220, 387–401.

Griffon-Etienne, G., Boucher, Y., Brekken, C., Suit, H.D., Jain, R.K., 1999. Taxane-induced apoptosis decompresses blood vessels and lowers interstitial fluid pressure in solid tumors: clinical implications. Cancer Res 59, 3776–3782.

Hanahan, D., Folkman, J., 1996. Patterns and emerging mechanisms of the angiogenic switch during tumorigenesis. Cell 86, 353–364.

Hashizume, H., Baluk, P., Morikawa, S., McLean, J.W., Thurston, G., Roberge, S., Jain, R.K., McDonald, D.M., 2000. Openings between defective endothelial cells explain tumor vessel leakiness. Am. J. Pathol. 156, 1363–1380.

Helmlinger, G., Netti, P.A., Lichtenbeld, H.C., Melder, R.J., Jain, R.K., 1997. Solid stress inhibits the growth of multicellular tumor spheroids. Nat. Biotechnol. 15, 778–783.

Hirst, D.G., Denekamp, J., Hobson, B., 1982. Proliferation studies of the endothelial and smooth-muscle cells of the mouse mesentery after irradiation. Cell Tissue Kinet 15, 251–261.

Hlatky, L., Hahnfeldt, P., Folkman, J., 2002. Clinical application of antiangiogenic therapy: microvessel density, what it does and doesn't tell us. J. Nat. Cancer Inst. 94, 883–893.

Holash, J., Maisonpierre, P.C., Compton, D., Boland, P., Alexander, C.R., Zagzag, D., Yancopoulos, G.D., Wiegand, S.J., 1999a. Vessel cooption, regression, and growth in tumors mediated by angiopoietins and VEGF. Science 284, 1994–1998.

Holash, J., Wiegand, S.J., Yancopoulos, G.D., 1999b. New model of tumor angiogenesis: dynamic balance between vessel regression and growth mediated by angiopoietins and VEGF. Oncogene 18, 5356–5362.

Ishida, T., Takahashi, M., Corson, M.A., Berk, B.C., 1997. Fluid shear stress-mediated signal transduction: how do endothelial cells transduce mechanical force into biological responses? ANN. Y. Acad. Sci. 811, 12–24.

Iyer, N.V., Kotch, L.E., Agani, F., Leung, S.W., Laughner, E., Wenger, R.H., Gassmann, M., Gearhart, J.D., Lawler, A.M., Yu, A.Y., Semenza, G.L., 1998. Cellular and developmental control of O-2 homeostasis by hypoxia-inducible factor 1 alpha. Genes Dev 12, 149–162.

Jimenez, B., Volpert, O.V., Crawford, S.E., Febbraio, M., Silverstein, R.L., Bouck, N., 2000. Signals leading to apoptosis-dependent inhibition of neovascularization by thrombospondin-1. Nat. Med. 6, 41–48.

Lee, D.S., Rieger, H., Bartha, K., 2006. Flow correlated percolation during vascular remodeling in growing tumors. Phys. Rev. Lett. 96, 058104-1–058104-4.

Levine, H.A., Pamuk, S., Sleeman, B.D., Nilsen-Hamilton, M., 2001. Mathematical modeling of capillary formation and development in tumor angiogenesis: penetration into the stroma. Bull. Math. Biol. 63, 801–863.

Lyden, D., Hattori, K., Dias, S., Costa, C., Blaikie, P., Butros, L., Chadburn, A., Heissig, B., Marks, W., Witte, L., Wu, Y., Hicklin, D., Zhu, Z.P., Hackett, N.R., Crystal, R.G., Moore, M.A.S., Hajjar, K.A., Manova, K., Benezra, R., Rafii, S., 2001. Impaired recruitment of bone-marrow-derived endothelial and hematopoietic precursor qcells blocks tumor angiogenesis and growth. Nat. Med. 7, 1194–1201.

Mandelbrot, B.B., 1983. The Fractal Geometry of Nature. W. H. Freeman, New York.

Maisonpierre, P.C., Suri, C., Jones, P.F., Bartunkova, S., Wiegand, S., Radziejewski, C., Compton, D., McClain, J., Aldrich, T.H., Papadopoulos, N., Daly, T.J., Davis, S., Sato, T.N., Yancopoulos, G.D., 1997. Angiopoietin-2, a natural antagonist for Tie2 that disrupts in vivo angiogenesis. Science 277, 55–60.

Maxwell, P.H., Dachs, G.U., Gleadle, J.M., Nicholls, G.L., Harris, A.L., Stratford, I.J., Hankinson, O., Pugh, C.W., Ratcliffe, P.J., 1997. Hypoxia-inducible factor-1 modulates gene expression in solid tumors and influences both angiogenesis and tumor growth. Proc. Natl. Acad. Sci. USA 94, 8104–8109.

McDougall, S.R., Anderson, A.R.A., Chaplain, M.A.J., Sherratt, J.A., 2002. Mathematical modeling of flow through vascular networks: Implications for tumor-induced angiogenesis and chemotherapy strategies. Bull. Math. Bio. 64, 673–702.

Milkiewicz, M., Brown, M.D., Egginton, S., Hudlicka, O., 2001. Association between shear stress, angiogenesis, and VEGF in skeletal muscles in vivo. Microcirculation 8, 229–241.

Minchenko, A., Leshchinsky, I., Opentanova, I., Sang, N.L., Srinivas, V., Armstead, V., Caro, J., 2002. Hypoxia-inducible factor-1-mediated expression of the 6-phosphofructo-2-kinase/fructose-2,6-bisphosphatase-3 (PFKFB3) gene—its possible role in the Warburg effect. J. Biol. Chem. 277, 6183–6187.

Nehls, V., Herrmann, R., Huhnken, M., 1998. Guided migration as a novel mechanism of capillary network remodeling is regulated by basic fibroblast growth. Histochem. Cell Biol. 109, 319–329.

O'Reilly, M.S., Holmgren, L., Shing, Y., Chen, C., Rosenthal, R.A., Moses, M., Lane, W.S., Cao, Y.H., Sage, E.H., Folkman, J., 1994. Angiostatin—a novel angiogenesis inhibitor that mediates the suppression of metastatses by a Lewis lung-carcinoma. Cell 79, 315–328.

O'Reilly, M.S., Boehm, T., Shing, Y., Fukai, N., Vasios, G., Lane, W.S., Flynn, E., Birkhead, J.R., Olsen, B.R., Folkman, J., 1997. Endostatin: an endogenous inhibitor of angiogenesis and tumor growth. Cell 88, 277–285.

Paku, S., 1998. Current concepts of tumour-induced angiogenesis. Pathol. Oncol. Res. 4, 62–75.

Plate, K.H., Risau, W., 1995. Angiogenesis in malignant gliomas. Glia 15, 339–347.

Plate, K.H., Breier, G., Weich, H.A., Risau, W., 1992. Vascular endothelial growth-factor is a potential tumor angiogenesis factor in human gliomas invivo. Nature 359, 845–848.

Pries, A.R., Secomb, T.W., Gaehtgens, P., 1995. Design principles of vascular beds. Circ. Res. 77, 1017–1022.

Ramanujan, S., Koenig, G.C., Padera, T.P., Stoll, B.R., Jain, R.K., 2000. Local imbalance of proangiogenic and antiangiogenic factors: a potential mechanism of focal necrosis and dormancy in tumors. Cancer Res 60, 1442–1448.

Risau, W., 1997. Mechanisms of angiogenesis. Nature 386, 671–674.

Secomb, T.W., Hsu, R., Park, E.Y.H., Dewhirst, M.W., 2004. Green's function methods for analysis of oxygen delivery to tissue by microvascular networks. Ann. Biomed. Eng. 32, 1519–1529.

Semenza, G.L., 2003. Targeting HIF-1 for cancer therapy. Nat. Rev. Cancer 3, 721–732.

Shweiki, D., Itin, A., Soffer, D., Keshet, E., 1992. Vascular endothelial growth-factor induced by hypoxia may mediate hypoxia-initiated angiogenesis. Nature 359, 843–845.

Stauffer, D., Aharony, A., 1992. Introduction to Percolation Theory, second ed. Taylor & Francis, London.

Tarjan, R., 1972. Depth-first search and linear graph algorithms. SIAM J. Comput. 1, 146–160.

Thompson, W.D., Shiach, K.J., Fraser, R.A., Mcintosh, L.C., Simpson, J.G., 1987. Tumors acquire their vasculature by vessel incorporation, not vessel ingrowth. J. Path. 151, 323–332.

Van Kampen, N.G., 1992. Stochastic processes in physics and chemistry. North Holland, Amsterdam.

Yu, J.L., Rak, J.W., Coomber, B.L., Hicklin, D.J., Kerbel, R.S., 2002. Effect of p53 status on tumor response to antiangiogenic therapy. Science 295, 1526–1528.

Zhou, M., Sutliff, R.L., Paul, R.J., Lorenz, J.N., Hoying, J.B., Haudenschild, C.C., Yin, M.Y., Coffin, J.D., Kong, L., Kranias, E.G., Luo, W.S., Boivin, G.P., Duffy, J., Pawlowski, S.A., Doetschman, T., 1998. Fibroblast growth factor 2 control of vascular tone. Nat. Med. 4, 201–207.